Mitigating Duty Cycle Limitation and Maximizing DC Voltage Gain in Switch Mode Power Supplies Utilizing Tapped-Inductor Topology: A Case Study with Buck Converter Analysis

Cagfer Yanarates and Aytac Altan

Abstract—**This paper presents a comparative analysis of tapped inductor (TI) buck converters versus conventional buck converter topologies, highlighting the advantages of TI buck converters. The primary motivations for using TI DC-DC converters in step-down applications, such as battery charging and photovoltaic emulator design, include significant input-to-output voltage differences resulting in low converter duty cycles, favorable peak-to-average current ratios, and overall conversion efficiency. In conventional buck converters, the DC voltage gain is determined solely by the duty cycle, leading to linear output voltage variation with the duty cycle for a given input voltage. In contrast, the DC voltage gain of TI buck converters depends on both the duty cycle and the turns ratio. While the operating principles of conventional and TI buck converters are similar, the TI topology offers a wider range of voltage step-down options based on the TI turns ratio. System characteristics are analyzed using the transfer function model for ease of use and pole-zero detection. The state-space averaging method, known for its simplicity, is applied with AC small signal analysis to derive transfer functions for both converter types. The results show that the use of a tapped rather than a conventional inductor does not alter the step-down characteristics of the conventional buck converter. Moreover, any DC voltage gain consistent with the conventional buck converter condition can be achieved at any duty cycle value by appropriate selection of the turn's ratio, increasing flexibility in converter design.**

Cağfer Yanarateş, is with Department of Electrical and Energy, Kelkit Aydın Doğan Vocational School, Gümüşhane University, Gümüşhane, Turkey, (e-mail: cagferyanarates@gumushane.edu.tr).

https://orcid.org/0000-0003-0661-0654

Aytaç Altan, is with Department of Electrical Electronics Engineering, Zonguldak Bülent Ecevit University, Zonguldak, Turkey, (e-mail: aytacaltan@beun.edu.tr).

https://orcid.org/0000-0001-7923-4528

I. INTRODUCTION

RECENTLY, THERE has been a growing demand for high efficiency voltage conversion with extreme step-down ratios in power electronics applications such as high frequency control systems, battery charging and renewable energy conversion technologies [1-3]. Particularly in buck converters, these ratios often result in excessively high or low duty cycles, adversely affecting both steady-state and transient performance [4, 5]. Due to limitations in the minimum pulse lengths of MOSFET gate drivers, small duty cycles can degrade power efficiency and transient dynamics [6-8]. One possible approach to address these issues is to use of transformers to increase the duty cycle. This approach offers benefits such as flexible converter duty cycles and the avoidance of extreme step-down ratios by selecting an appropriate turn ratio (λ) [9]. This flexibility reduces peak currents, switching losses, and conduction losses [10]. However, considering the transformer losses and increased size due to additional reset components, isolation-type converters have lower efficiency. Tapped inductor (TI) applications have attracted interest because they allow extreme voltage conversion with high efficiency [11, 12]. TIs use less copper than isolation transformers and function as autotransformers without the need for a reset circuit [13].

DC-DC converter product datasheets typically provide comprehensive information on the operating ranges for both input and output voltages [14]. These ranges are often presented as wide and occasionally overlapping, providing the user with a degree of flexibility [15]. However, despite the wide range of acceptable input voltages, it is often not possible to derive an arbitrary output voltage. This limitation is due to various factors inherent in the design and operation of the converter [16]. These factors include the internal reference voltage, which serves as a critical reference point for the converter's operation, the minimum controlled ON time, which determines the minimum amount of time the converter's switches can remain in the ON state, and the maximum duty cycle limits, which dictate the upper limit for the ratio of ON time to total switching time [17, 18]. Together, these constraints limit the output voltage range that can be achieved and require careful consideration during the design and selection process for DC-DC converters [19, 20].

This paper presents a tapped inductor-based DC-DC buck converter designed for photovoltaic (PV) emulation, specifically replicating the characteristics of the 1Soltech 1STH-215-P PV module. A comprehensive comparative analysis with conventional buck converters is performed. System characteristics and behaviour are investigated using the state space averaging method along with AC small signal analysis to derive transfer functions for both conventional and TI buck converters.

The remainder of the paper is organized as follows: Section II introduces the proposed tapped inductor DC-DC buck converter-based PV emulator. Section III presents the simulation results and analysis. Finally, Section IV emphasizes the study's conclusions.

II. PROPOSED TAPPED INDUCTOR DC-DC BUCK CONVERTER BASED PV EMULATOR

The main motivations for using a TI DC-DC buck converter-based PV emulator are the significant input-to-output voltage differences that result in very low converter duty cycles, improved peak-to-average current ratios and improved overall conversion efficiency. Although the operating principles of conventional and TI buck converters are similar, the TI topology offers a wide range of voltage step-down depending on the TI turn ratio (λ). The large difference between the input and output voltages is a challenge for conventional buck converters due to the resulting very low duty cycles. The conventional and TI buck converter topologies are shown in Fig. 1.
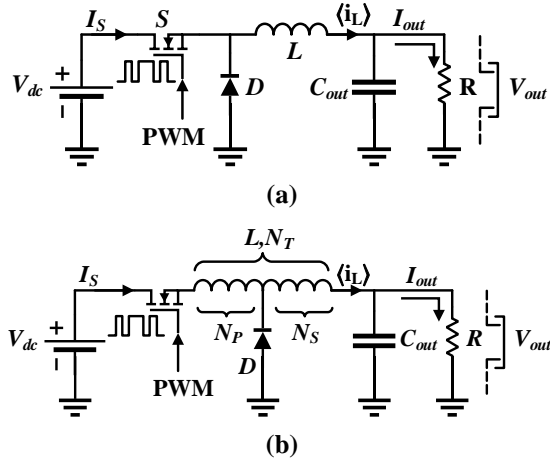

(a)

(b)

Fig.1. Circuit topologies of PWM DC-DC buck converter **a)** conventional **b)** TI.

The buck converter consists of a power source (V_{dc}), two switches (S and D), an inductor (L), a filter capacitor (C_{out}), and a load (R) as shown in the Fig. 1. The basic operation of the buck converter is based on current control in the inductor by two switches: an active switch, typically a MOSFET (S), and a passive switch, typically a diode (D). The purpose of the filter capacitor is to reduce the voltage ripple across the load. The inductor L is switched on and off by applying a control signal to the gate of the MOSFET. The control and switching signals are illustrated in Fig. 2.
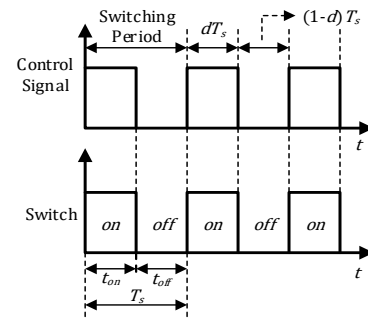

Fig.2. Control and switching signals for the MOSFET gate to reduce load voltage ripple using the filter capacitor.

The turn ratio λ is determined by

$$\lambda = \frac{N_T}{N_S} = \frac{N_P + N_S}{N_S} \tag{1}$$

where N_T, N_P, and N_S are the total number of windings, the number of primary windings and the number of secondary windings respectively.

Since it is possible to implement suitable variations of λ that include both cases $N_T > N_S$ and $N_T < N_S$, the equations that define the behaviour of the converter are the same in both cases. However, the total inductance value of the tapped inductor, which refers to the turn-on inductance, is different in the two cases and is calculated as

$$N_T > N_S \Rightarrow L_{Total} = L \tag{2}$$

$$N_T < N_S \Rightarrow L_{Total} = L/\lambda^2 \tag{3}$$

The current waveforms of the inductor for both conventional and TI DC-DC buck converters are depicted in Fig. 3.
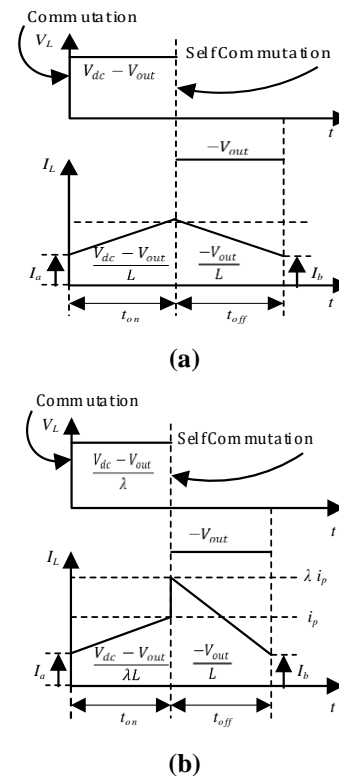

(a)

(b)

Fig.3. Inductor current waveforms for **a)** conventional and **b)** TI DC-DC buck converters.

The increase in the inductor current I_L during the on-state (time interval: $0 < t < dT_s$) for a conventional buck converter is given by

$$\Delta I_{L(on)} = \int_0^{t_{on}} \frac{V_L}{L} dt = \frac{V_{dc} - V_{out}}{L} t_{on} \qquad (4)$$

$$t_{on} = dT_s \qquad (5)$$

where V_L, d, and T_s are the inductor voltage, duty cycle and switching time respectively. Conversely, for a conventional buck converter, the decrease in inductor current during the off-state (time interval: $dT_s < t < T_s$) is given by

$$\Delta I_{L(off)} = \int_{t_{on}}^{T_s = t_{on} + t_{off}} \frac{V_L}{L} dt = \frac{-V_{out}}{L} t_{off} \qquad (6)$$

$$t_{off} = (1 - d)T_s \qquad (7)$$

The increase in the inductor current during the on-state (time interval: $0 < t < dT_s$) for TI buck converters is expressed by

$$\Delta I_{L(on)} = \int_0^{t_{on}} \frac{V_L}{L} dt = \frac{V_{dc} - V_{out}}{\lambda L} t_{on} \qquad (8)$$

$$t_{on} = dT_s \qquad (9)$$

The decrease in the inductor current during the off-state (time interval: $dT_s < t < T_s$) for TI buck converters is given by:

$$\Delta I_{L(off)} = \int_{t_{on}}^{T_s = t_{on} + t_{off}} \frac{V_L}{L} dt = \frac{-V_{out}}{L} t_{off} \qquad (10)$$

$$t_{off} = (1 - d)T_s \qquad (11)$$

In steady-state operation, the energy stored in the inductor at the end of commutation is equal to the energy delivered during self-commutation, as shown in the Fig. 3. Accordingly, the steady-state inductor current equation can be written as

$$\Delta I_{L(on)} + \Delta I_{L(off)} = 0 \qquad (12)$$

$$\frac{V_{dc} - V_{out}}{L} t_{on} - \frac{V_{out}}{L} t_{off} = 0 \qquad (13)$$

$$\frac{V_{out}}{V_{dc}} = d \ (for\ conventional\ buck\ converter) \qquad (14)$$

$$\frac{V_{dc} - V_{out}}{\lambda L} t_{on} - \frac{V_{out}}{L} t_{off} = 0 \implies \qquad (15)$$

$$\frac{V_{out}}{V_{dc}} = \frac{d}{d + \lambda(1 - d)} \ (for\ TI\ buck\ converter) \qquad (16)$$

The DC voltage gain for the conventional buck converter is a function of the duty cycle alone, with the output voltage varying linearly with the duty cycle for a given input voltage. In contrast, the DC voltage gain for the TI buck converter depends on both the duty cycle and the turns ratio. The DC voltage gain plot for the TI buck converter is shown in the Fig. 4.
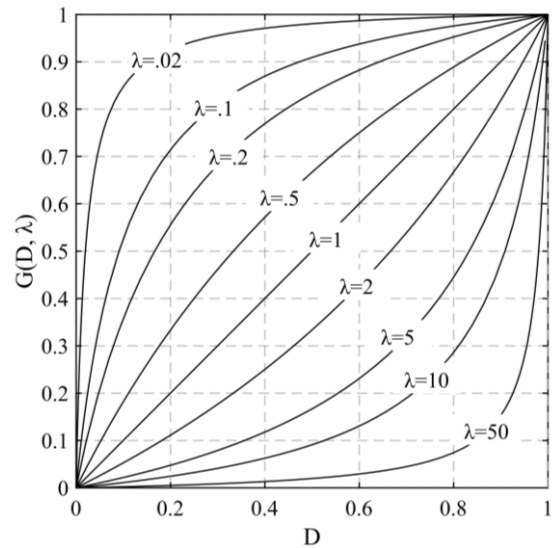

Fig.4. DC voltage gain plot for TI buck converter as a function of duty cycle and turns ratio.

A. Derivation of the Transfer Functions

A transfer function, typically represented in the s-domain, is a mathematical model that describes the relationship between the input and output signals of a system as determined by the physical characteristics of the system. This model is advantageous for analyzing the characteristics and behaviour of the system because it simplifies the equations by eliminating differential terms and allows easy identification of pole-zero locations. The state-space averaging method is used to derive the transfer functions of both conventional and TI buck converters. Its ease of derivation and implementation, together with the significant insights it provides, make the state-space averaging method an invaluable and practical tool in power electronics applications.

The state variables for the system include the inductor current (i_L) and the capacitor voltage (V_C) because the inductor and capacitor are the only energy storage components in the buck converter. Consequently, the state vector x for the buck converter is defined as

$$x = \begin{bmatrix} i_L \\ V_C \end{bmatrix} \qquad (17)$$

The state-space averaging equations for a conventional asynchronous buck converter, excluding parasitic resistances, are presented as:

On-time system matrix A_1:

$$A_1 = \begin{bmatrix} 0 & \dfrac{-1}{L} \\ \dfrac{1}{C_{out}} & \dfrac{-1}{RC_{out}} \end{bmatrix} \qquad (18)$$

Off-time system matrix A_2:

$$A_2 = \begin{bmatrix} 0 & \dfrac{-1}{L} \\ \dfrac{1}{C_{out}} & \dfrac{-1}{RC_{out}} \end{bmatrix} \qquad (19)$$

The averaged system matrix A:

$$A = \begin{bmatrix} 0 & \dfrac{-1}{L} \\ \dfrac{1}{C_{out}} & \dfrac{-1}{RC_{out}} \end{bmatrix} \tag{20}$$

On-time input matrix B_1:

$$B_1 = \begin{bmatrix} \dfrac{1}{L} \\ 0 \end{bmatrix} \tag{21}$$

Off-time input matrix B_2:

$$B_2 = \begin{bmatrix} 0 \\ 0 \end{bmatrix} \tag{22}$$

The average input matrix B:

$$B = \begin{bmatrix} \dfrac{D}{L} \\ 0 \end{bmatrix} \tag{23}$$

Average state-space equation:

$$\dot{x} = Ax + BV_{dc} \tag{24}$$

$$\begin{bmatrix} \dfrac{di_L}{dt} \\ \dfrac{dV_C}{dt} \end{bmatrix} = \begin{bmatrix} 0 & \dfrac{-1}{L} \\ \dfrac{1}{C_{out}} & \dfrac{-1}{RC_{out}} \end{bmatrix} \begin{bmatrix} i_L \\ V_C \end{bmatrix} + \begin{bmatrix} \dfrac{D}{L} \\ 0 \end{bmatrix} [V_{dc}] \tag{25}$$

The state space averaging equations for TI asynchronous buck converters without consideration of parasitic resistances are as follows:

On-time system matrix A_1:

$$A_1 = \begin{bmatrix} 0 & \dfrac{-1}{L} \\ \dfrac{1}{C_{out}} & \dfrac{-1}{RC_{out}} \end{bmatrix} \tag{26}$$

Off-time system matrix A_2:

$$A_2 = \begin{bmatrix} 0 & \dfrac{-\lambda}{L} \\ \dfrac{\lambda}{C_{out}} & \dfrac{-1}{RC_{out}} \end{bmatrix} \tag{27}$$

The averaged system matrix A:

$$A = \begin{bmatrix} 0 & \dfrac{-1}{L}[D + (1-D)\lambda] \\ \dfrac{1}{C_{out}}[D + (1-D)\lambda] & \dfrac{-1}{RC_{out}} \end{bmatrix} \tag{28}$$

On-time input matrix B_1:

$$B_1 = \begin{bmatrix} \dfrac{1}{L} \\ 0 \end{bmatrix} \tag{29}$$

Off-time input matrix B_2:

$$B_2 = \begin{bmatrix} 0 \\ 0 \end{bmatrix} \tag{30}$$

The average input matrix B:

$$B = \begin{bmatrix} \dfrac{D}{L} \\ 0 \end{bmatrix} \tag{31}$$

Average state-space equation:

$$\dot{x} = Ax + BV_{dc} \tag{32}$$

$$\begin{bmatrix} \dfrac{di_L}{dt} \\ \dfrac{dV_C}{dt} \end{bmatrix} = \begin{bmatrix} 0 & \dfrac{-1}{L}[D + (1-D)\lambda] \\ \dfrac{1}{C_{out}}[D + (1-D)\lambda] & \dfrac{-1}{RC_{out}} \end{bmatrix} \begin{bmatrix} i_L \\ V_C \end{bmatrix} + \begin{bmatrix} \dfrac{D}{L} \\ 0 \end{bmatrix} [V_{dc}] \tag{33}$$

The state-space equations obtained after the averaging process define the behaviour of the converters. In the case of unity turns ratio ($\lambda = 1$), both converters have the same dynamic behaviour.

B. AC Small Signal Analysis

AC small signal analysis of converters involves deriving the averaged state-space equations and superimposing an AC variation (perturbation) around the steady state point. To determine the steady state operating point of the system, the time derivative in the state equation is set to zero. To highlight the steady-state operating point, the state equation is expressed using capital letters for the state variable vector as follows:

$$AX + BV_{dc} = 0 \tag{34}$$

The state variable vector X for steady-state operation in a conventional buck converter is obtained as follows:

$$X = (sI - A)^{-1}BU \tag{32}$$

$$-A^{-1}BV_{dc} = -\dfrac{adj\begin{bmatrix} 0 & \dfrac{-1}{L} \\ \dfrac{1}{C_{out}} & \dfrac{-1}{RC_{out}} \end{bmatrix}\begin{bmatrix} \dfrac{D}{L} \\ 0 \end{bmatrix}}{det\begin{bmatrix} 0 & \dfrac{-1}{L} \\ \dfrac{1}{C_{out}} & \dfrac{-1}{RC_{out}} \end{bmatrix}} V_{dc} \tag{33}$$

$$-A^{-1}BV_{dc} = \begin{bmatrix} \dfrac{DV_{dc}}{R} \\ DV_{dc} \end{bmatrix} \tag{34}$$

Response to the variation in duty cycle in terms of state variables is written as:

$$\dfrac{\hat{x}(s)}{\hat{d}(s)} = (sI - A)^{-1}[(A_1 - A_2)X + (B_1 - B_2)V_{dc}] \tag{35}$$

Duty ratio to inductor current transfer function for the conventional buck converter is given as:

$$\dfrac{\hat{x}(s)}{\hat{d}(s)} = \dfrac{\begin{bmatrix} \hat{i}_L \\ \hat{V}_C \end{bmatrix}}{\hat{d}(s)} = \begin{bmatrix} \dfrac{V_{dc}(C_{out}Rs + 1)}{C_{out}LRs^2 + Ls + R} \\ \dfrac{V_{dc}R}{C_{out}LRs^2 + Ls + R} \end{bmatrix} \tag{36}$$

$$\frac{i_L(s)}{d(s)} = \frac{V_{dc}}{L} \cdot \frac{s + \frac{1}{RC_{out}}}{s^2 + \frac{s}{RC_{out}} + \frac{1}{LC_{out}}} \qquad (37)$$

The state variable vector X in steady-state operation is obtained for the TI buck converter as follows:

$$X = (sI - A)^{-1}BU \qquad (38)$$

$$X = -A^{-1}BV_{dc} \qquad (39)$$

$$X = -\frac{adj \begin{bmatrix} 0 & \frac{-1}{L}[D+(1-D)\lambda] \\ \frac{1}{C_{out}}[D+(1-D)\lambda] & \frac{-1}{RC_{out}} \end{bmatrix}}{det \begin{bmatrix} 0 & \frac{-1}{L}[D+(1-D)\lambda] \\ \frac{1}{C_{out}}[D+(1-D)\lambda] & \frac{-1}{RC_{out}} \end{bmatrix}} \begin{bmatrix} \frac{D}{L} \\ 0 \end{bmatrix} V_{dc} \qquad (40)$$

$$X = \begin{bmatrix} \frac{DV_{dc}}{R(D+(1-D)\lambda)^2} \\ \frac{DV_{dc}}{D+(1-D)\lambda} \end{bmatrix} \qquad (41)$$

The duty cycle to inductor current transfer function for the TI buck converter is as follows:

$$\frac{\hat{x}(s)}{\hat{d}(s)} = \begin{bmatrix} \hat{\imath}_L \\ \hat{V}_C \end{bmatrix} = \begin{bmatrix} \frac{L\sigma_2(C_{out}Rs+1)}{\sigma_1} + \frac{DV_{dc}(\lambda-1)}{\sigma_3\sigma_1} \\ \frac{LR\sigma_2\sigma_3}{\sigma_1} - \frac{DLV_{dc}s(\lambda-1)}{\sigma_3{}^2\sigma_1} \end{bmatrix} \qquad (42)$$

where

$$\sigma_1 = RD^2\lambda^2 - 2RD^2\lambda + RD^2 - 2RD\lambda^2 + 2RD\lambda \\ + C_{out}LRs^2 + Ls + R\lambda^2 \qquad (43)$$

$$\sigma_2 = \frac{V_{dc}}{L} + \frac{DV_{dc}(\lambda-1)}{L\sigma_3} \qquad (44)$$

$$\sigma_3 = D + (1-D)\lambda \qquad (45)$$

The numerator and denominator equations of the duty cycle to inductor current transfer function $(i_L(s)/d(s))$ for the TI buck converter are given as

Numerator:

$$V_{dc}(C_{out}R\lambda s + \lambda - D + D\lambda) \qquad (46)$$

Denominator:

$$C_{out}LR[D+(1-D)\lambda]s^2 + L[D+(1-D)\lambda]s + [D \\ + (1-D)\lambda]\sigma_4 \qquad (47)$$

where

$$\sigma_4 = RD^2\lambda^2 - 2RD^2\lambda + RD^2 - 2RD\lambda^2 + 2RD\lambda + R\lambda^2 \qquad (48)$$

C. Calculations the Values of Buck Converter-based PVE Components

A switch topology known as a "buck converter" converts a DC input voltage (V_{in}) to a DC output voltage (V_{out}) where the output voltage is always less than the input voltage ($V_{out} < V_{in}$). The lower switch in an asynchronous buck converter is implemented by a diode which automatically turns on when the upper switch - implemented by an IGBT or MOSFET - is turned off. An asynchronous buck converter is typically designed to operate in continuous current mode (CCM), where the operating range is chosen so that the diode is always forward biased and the inductor current is always positive. The equations that characterize the behaviour of the converter change when this requirement is not met. Two different states of the switched mode topology of the CCM are shown in Fig. 1. The controllable switch (S) is activated and connects the input voltage to the LC circuit that drives the inductor current when the control signal is high. This is maintained for a set time, known as the on-time (t_{on}), after which the control signal switches to a low state, turning off the controllable switch and driving current through the diode. This is maintained for a period known as the off time (t_{off}).

The steady-state duty cycle of the system is represented as follows:

$$D = \frac{V_{out}}{V_{in}} \qquad (49)$$

The maximum average current through the inductor is given by

$$I_{L,avg,max} = \frac{V_{out}}{R_{min}} \qquad (50)$$

The peak-to-peak inductor ripple current, which is 20% of the average inductor current, is shown as

$$\Delta I_L = 0.2 \times I_{L,avg,max} \qquad (51)$$

The inductance value L of the inductor is given by

$$L = \frac{V_{in}(1-D)D}{f_{sw}\Delta I_L} \qquad (52)$$

The capacitor voltage ripple ΔV_C or output voltage ripple ΔV_{out}, which is $\pm 2\%$ of the average output voltage, is represented as

$$\Delta V_C = \Delta V_{out} = 0.04 \times V_{out} \qquad (53)$$

The capacitance value C of the capacitor is given by

$$C = \frac{V_{in}(1-D)D}{8Lf_{sw}{}^2\Delta V_C} \qquad (54)$$

The computed values of the PVE parameters and components are listed in Table I.

TABLE I
COMPUTED VALUES OF THE PVE PARAMETERS AND COMPONENTS

Parameters and Components	**Value**
Steady-state duty cycle (D)	0.6042
Maximum average inductor current (A)	7.3483
Maximum average inductor current ripple (A)	1.4697
Inductor value (mH)	0.781
Output voltage ripple (V)	1.16
Capacitor value (μF)	15.837

The duty ratio to the inductor current transfer function for the conventional buck converter topology is obtained from Eq. 56 by substituting the calculated component values in Table I for the intended emulator as follows:

$$G_{conv}(s) = \frac{i_L(s)}{d(s)} = \frac{V_{in}}{L} \frac{s + \frac{1}{RC_{out}}}{s^2 + \frac{s}{RC_{out}} + \frac{1}{LC_{out}}} \qquad (55)$$

$$G_{conv}(s) = (6.1455e4) \frac{s + 1.6e4}{s^2 + 1.6e4s + 8.0841e7} \qquad (56)$$

The duty ratio to the inductor current transfer function is derived from Eq. 58 for the TI buck converter topology by substituting of the calculated component values from Table I for the intended emulator in steady-state operation with an arbitrarily selected $\lambda = 3$ and corresponding $D = 0.821$ as:

$$G_{tap}(s) = \frac{V_{in}}{R} \frac{sRC_{out} + 1}{s^2LC_{out} + s\left(\frac{L}{R}\right) + (D + (1 - D)\lambda)^2)} \qquad (57)$$

$$G_{tap}(s) = (6.1455e4) \frac{s + 1.6e4}{s^2 + 1.6e4s + 1.5e8} \qquad (58)$$

Step responses of both transfer functions with scaling factors of 0.08 for $G_{conv}(s)$ and 0.15 for $G_{tap}(s)$ are shown in Fig. 5.
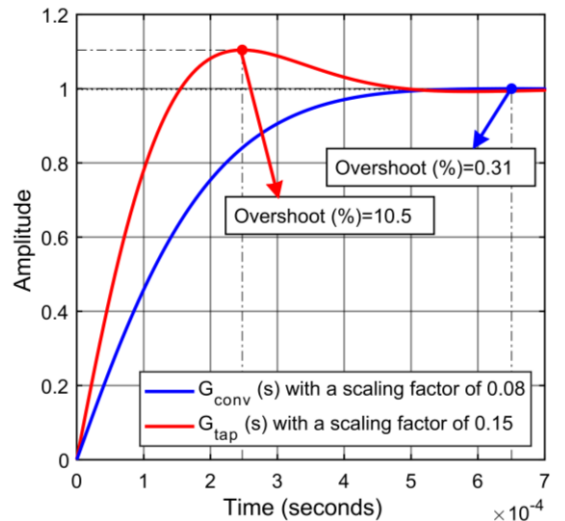

Fig.5. Step responses of both transfer functions with scaling factors of 0.08 for $G_{conv}(s)$ and 0.15 for $G_{tap}(s)$.

It can be concluded from the step responses that the same output is generated by implementing duty cycles of 0.6042 for $G_{conv}(s)$ and 0.821 for $G_{tap}(s)$. The open-loop step response characteristics of the derived transfer functions $G_{conv}(s)$ and $G_{tap}(s)$ are presented in Table II.

TABLE II
OPEN-LOOP STEP RESPONSE CHARACTERISTICS FOR $G_{conv}(s)$
AND $G_{tap}(s)$

Step Response Characteristics	Conventional Buck Converter	TI Buck Converter
Rise Time (s)	2.7203e-04	1.1457e-04
Settling Time (s)	4.1803e-04	4.2600e-04
Settling Minimum	10.9681	5.9717
Settling Maximum	12.2004	7.2888
Overshoot (%)	0.3100	10.5159
Undershoot	85.1766	81.2702
Peak	12.2004	7.2888
Peak Time (s)	6.5048e-04	2.4753e-04

The use of a tapped inductor does not affect the step-down characteristics of a traditional buck converter; for example, if a buck converter is used for any ratio of N_T and N_S (for any λ), the output voltage will be lower than the input voltage.

If the appropriate ratio N_T/N_S is chosen, any DC voltage gain can be obtained at any duty cycle value, consistent with the conventional buck converter condition. This allows more flexibility in the converter design. In CCM, the turns ratio has a significant effect on the dynamic response of the system. The poles of the TI buck converter are located in:

$$s_{TI,buck} = \frac{-L\tau_1 \pm \sqrt{L\tau_1^2 - 4C_{out}LR\tau_1^2\tau_2}}{2C_{out}LR\tau_1} \qquad (59)$$

where

$$\tau_1 = [D + (1 - D)\lambda] \qquad (60)$$

$$\tau_2 = RD^2\lambda^2 - 2RD^2\lambda + RD^2 - 2RD\lambda^2 + 2RD\lambda + R\lambda^2 \qquad (61)$$

The zeros of the TI buck converter are located in:

$$z_{TI,buck} = -\frac{1}{C_{out}R}\left(\frac{\lambda + \lambda D - D}{\lambda}\right) \qquad (62)$$

The values of $(\lambda + \lambda D - D)/\lambda$ versus the corresponding values of λ is plotted in Fig. 6.
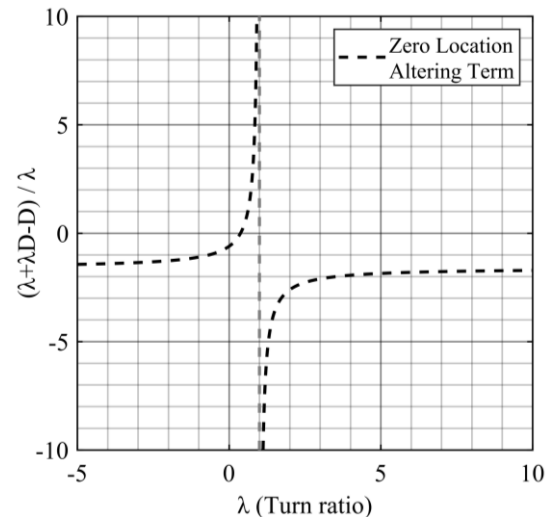

Fig.6. Plot of the relationship between λ and its corresponding values, showing the zero location of the TI buck converter transfer function.

Fig. 6 shows that the zero point of the TI buck converter transfer function is located in different regions of the complex plane depending on the value of λ.

Equivalent inductance L_{eq} of the TI buck converter is given in:

$$L_{eq} = \frac{L}{[D + (1 - D)\lambda]^2} \qquad (63)$$

Eqs. (59) and (63) denotes that L_{eq} and the pole locations of the TI buck converter are a function of λ. An increase in the value of λ leads to decrease in L_{eq} and consequently the system produces a more oscillatory response. The value of λ also affects the locations of the zeros in the transfer function of the TI buck converter. The locations of the poles and zeros as a function of varying λ for the TI buck converter are given in Fig. 7.
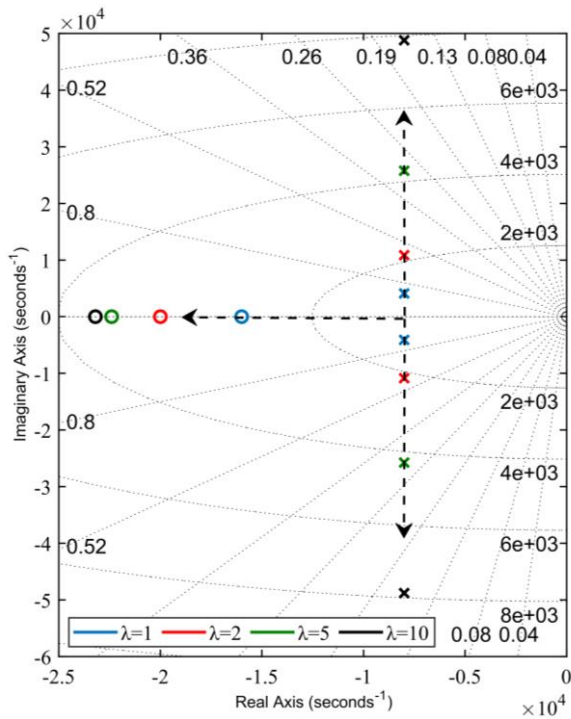
Fig.7. Pole and zero locations as a function of varying λ for the TI buck converter.

III. SIMULATION RESULTS AND ANALYSIS

In this study, two different tapped inductor circuit structures are used to demonstrate the performance of the proposed emulator under varying duty cycles compared to the conventional buck converter topology-based PV emulator. The tapped inductor structures are shown in Fig. 8.
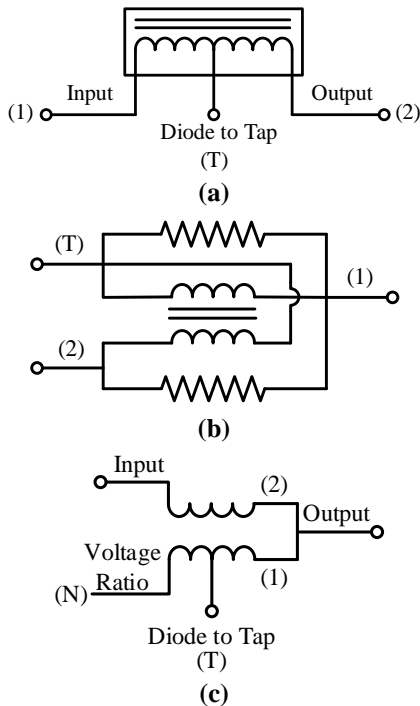

Fig.8. Proposed tapped inductor circuit structures a) generic representation of the TI structure b) mutual inductance-based TI c) variable-ratio transformer-based TI.

In the first structure, two inductances are implemented with mutual coupling. The inductance and resistance matrices are defined as

$$R = \begin{bmatrix} R_1 & R_m \\ R_m & R_2 \end{bmatrix} \quad and \quad L = \begin{bmatrix} L_1 & L_m \\ L_m & L_2 \end{bmatrix} \qquad (64)$$

R represents resistance, R_1 and R_2 are self-resistances, R_m is mutual resistance ($R_m <$ and R_2), L represents inductance, L_1 and L_2 are self-inductances, and L_m is mutual inductance ($L_m \leq \sqrt{L_1.L_2}$). Outstanding property of the structure is that an extra degree of freedom addition to the system and accordingly the input-output voltage relationship of the buck converter in CCM is transformed into the following:

$$\frac{V_{out}}{V_{in}} = D - \left(\frac{\lambda}{D \times (1-\lambda)} \right) \qquad (65)$$

where λ is the ratio of primary number of windings to total number of windings.

In the second structure, a discrete, variable-ratio, two-winding ideal transformer is used. Working principle of the structure is based on implementation of the primary winding as current source and secondary winding as a voltage source. Apart from the turn ratio, voltage ratio is applied, and it is defined as:

$$N = \frac{V_S}{V_P} \qquad (66)$$

The voltage at primary winding, denoted as V_P, relates to the voltage at secondary winding, denoted as V_S, through the principle of transformer action. The performance of the proposed buck converter topologies created with two different tapped inductor structures was compared with the conventional buck converter by reducing the duty cycle from 0.9 to 0.1 at 0.1 intervals. Accordingly, the obtained output voltages are given in Fig. 9.
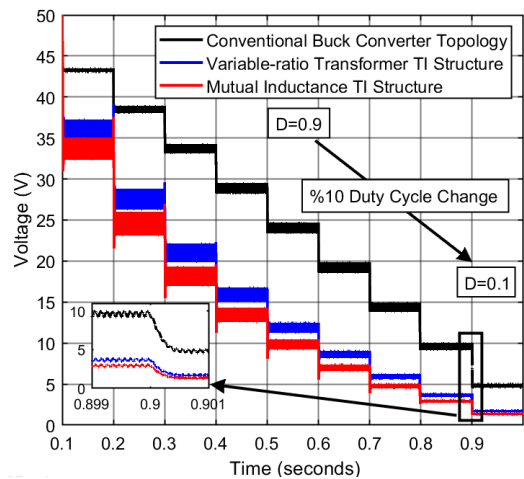

Fig.9. Performance assessment of proposed TI circuit topologies under varying duty cycles.

The results clearly show that the limitation in the duty cycle is eliminated by the TI structure, especially at very small values. To be more specific, while an input-output voltage ratio of 20% is achieved in a conventional buck converter with a duty cycle of 0.2, this ratio is approximately 3.5% with the TI structure with the same duty cycle.

IV. CONCLUSIONS

To highlight the advantages of TI buck converters, this paper has compared TI and conventional buck converter topologies. The results showed that the proposed TI buck converter achieved low converter duty cycles, favorable peak-to-average current ratios and overall conversion efficiency when faced with large input-to-output voltage differences. In contrast, the conventional buck converter produced a linear output voltage variation with the duty cycle for a given input voltage, as the DC voltage gain is solely determined by the duty cycle. On the other hand, the DC voltage gain of the TI buck converter is influenced by both the duty cycle and the turns ratio.

Although conventional and TI buck converters operate on similar principles, the TI topology offers more voltage step-down possibilities due to the TI turns ratio. The transfer function model is used to evaluate system characteristics for ease of use and easy pole zero identification. The transfer functions for both converter types are derived using the state space averaging method, which is known for its simplicity, together with AC small signal analysis. The results show that the step-down characteristics of the conventional buck converter remain unchanged when a tapped inductor is used instead of the standard inductor. Furthermore, by carefully selecting the turns ratio, any duty cycle value can be used to achieve any DC voltage gain consistent with the conventional buck converter state, significantly increasing the versatility of the converter design.

REFERENCES

[1] P. Azer, A. Emadi. "Generalized state space average model for multi-phase interleaved buck, boost and buck-boost DC-DC converters: Transient, steady-state and switching dynamics." IEEE Access, vol. 8, 2020, pp. 77735-77745.
[2] F. Musavi, W. Eberle. "Overview of wireless power transfer technologies for electric vehicle battery charging." IET Power Electronics, vol. 7, 1, 2014, pp. 60-66.
[3] Y. Wang, O. Lucia, Z. Zhang, Y. Guan, D. Xu. "Review of very high frequency power converters and related technologies." IET Power Electronics, vol. 13, 9, 2020, pp. 1711-1721.
[4] P. Alavi, E. Babaei, P. Mohseni, V. Marzang. "Study and analysis of a DC-DC soft-switched buck converter." IET Power Electronics, vol. 13, 7, 2020, pp. 1456-1465.
[5] G. M. Sung, C. T. Lee, Z. L. Chen. "Buck converter IC for brushless DC motor drive using voltage-mode PWM controller." IET Power Electronics, vol. 13, 12, 2020, pp. 2547–2554.
[6] A. Chadha, A. Ayachit, D. K. Saini, M. K. Kazimierczuk. "Steady-state analysis of PWM tapped-inductor buck DC-DC converter in CCM." IEEE Texas Power Energy Conference (TPEC), College Station, TX, USA, 2018.
[7] B. J. Tucker. "Understanding output voltage limitations of DC/DC buck converters." Analog Applications Journal, 2008, pp. 11–14.
[8] V. Michal. "Dynamic duty-cycle limitation of the boost DC/DC converter allowing maximal output power operations." International Conference on Applied Electronics (AE), Pilsen, Czech Republic, 2016.
[9] K. W. E. Cheng. "Tapped inductor for switched-mode power converters." 2nd International Conference on Power Electronics Systems and Applications, Hong Kong, China, 2006.
[10] N. Kondrath, M. K. Kazimierczuk. "Analysis and design of common-diode tapped-inductor PWM buck converter in CCM." Electrical Manufacturing and Coil Winding Conference, Nashville, TN, 2009.
[11] M. Rico, J. Uceda, J. Sebastian, F. Aldana. "Static and dynamic modeling of tapped-inductor DC-to-DC converters." IEEE Power Electronics Specialists Conference, Blacksburg, VA, USA, 1987.
[12] H. Tarzamni, N. V. Kurdkandi, H. S. Gohari, M. Lehtonen, O. Husev, F. Blaabjerg. "Ultra-high step-up DC-DC converters based on center-tapped inductors." IEEE Access, vol. 9, 2021, pp. 136373–136383.
[13] L. Wu, Y. Chen, S. Yang. "Design and research on tapped inductor of large step-up ratio DC/DC converter." IOP Conference Series: Earth and Environmental Science, vol. 617, 1, 2020, pp. 1-8.
[14] D. K. Saini, A. Chadha, A. Ayachit, A. Reatti, M. K. Kazimierczuk. "Duty cycle and input-to-output voltage transfer functions of tapped-inductor buck DC-DC converter." IEEE International Symposium on Circuits and Systems (ISCAS), Florence, Italy, 2018.
[15] J. H. Park, B. H. Cho. "Nonisolation soft-switching buck converter with tapped-inductor for wide-input extreme step-down applications." IEEE Transactions on Circuits and Systems I: Regular Papers, vol. 54, 8, 2007, pp. 1809-1818.
[16] C. S. Yeh, X. Zhao, J. S. Lai. "A MHz zero voltage switching (ZVS) tapped-inductor buck converter for wide-input high step-down low-power applications." IEEE 3rd International Future Energy Electronics Conference and ECCE Asia (IFEEC 2017-ECCE Asia), Kaohsiung, 2017.
[17] J. Yao, K. Li, K. Zheng, A. Abramovitz. "On the equivalence of the switched inductor and the tapped inductor converters and its application to small signal modelling." Energies, vol. 12, 24, 2019, 4806.
[18] D. A. Grant, Y. Darroman, J. Suter. "Synthesis of tapped-inductor switched-mode converters." IEEE Transactions on Power Electronics, vol. 22, 5, 2007, pp. 1964–1969.
[19] A. Chadha, M. K. Kazimierczuk. "Small-signal modeling of open-loop PWM tapped-inductor buck DC-DC converter in CCM." IEEE Transactions on Industrial Electronics, vol. 68, 7, 2021, pp. 5765-5775.
[20] S. Pal, B. Singh, A. Shrivastava. "High efficiency wide input extreme output (WIEO) tapped inductor buck-boost converter for high power LED lighting." IET Power Electronics, vol. 13, 3, 2020, pp. 535-544.

BIOGRAPHIES

CAĞFER YANARATEŞ received the M.Sc. degree in Power Engineering and Sustainable Energy FHEQ7 Taught Masters/PGDip/PGCert from Swansea University in 2017. He received his Ph.D. degree from the Department of Electrical and Electronics Engineering at the same university in 2022. He is currently an Assistant Professor in the Department of Electrical and Energy Engineering at Gümüşhane University, Kelkit Aydın Doğan Vocational High School in Turkey. He is mainly concerned with the application of power electronic converters in photovoltaic systems and their control.

AYTAÇ ALTAN received his B.Sc. and M.Sc. degrees in the department of Electrical Electronics Engineering from Anadolu University in 2004 and 2006, respectively. He is received his Ph.D. degree in the department of Electrical Electronics Engineering from Zonguldak Bülent Ecevit University in 2018. He is currently an Associate Professor at the department of Electrical Electronics Engineering at the Zonguldak Bülent Ecevit University in Turkey. His research interests include signal processing, image processing, optimization techniques, artificial intelligence, data mining, system identification, model-based control, and robotic systems.